JOURNAL OF MATERIALS SCIENCE 20 (1985) 1351–1356

Fracture characteristics of a burst tested maraging steel rocket motor case

V. DIWAKAR, S. ARUMUGHAM, T. S. LAKSHMANAN, B. K. SARKAR
Materials Group, Vikram Sarabhai Space Centre, Trivandrum 695 022, India

A 0.3 m diameter, 2 m long and 0.0015 m thick, 18 nickel 1800 MNm^{-2} grade maraging steel motor case was designed, fabricated and burst tested to gain experience for using the steel as booster case material in satellite launch vehicles. The bursting occurred at 15.2 MPa for which the effective hoop stress worked out to be 1754 MNm^{-2} almost equal to the ultimate tensile strength (1764 MNm^{-2}) of the material in the solution treated and aged condition. The failure analysis revealed that the material failed due to normal tensile overload fracture. The burst test data was used to arrive at fracture mechanics parameters like crack size, gross section area stress and the stress for leak before bursting.

1. Introduction

Maraging steels have such a useful combination of properties that they are already being used for many applications demanding high strength. Whilst the conventional carbon martensite alloy can equal the maraging steels for strength, the unique nickel martensite alloy system in a maraging steel provides superior ductility and toughness with improved resistance to crack propagation, particularly in corrosive environments. In aircraft applications considerable weight savings have been achieved by the use of maraging steel for structural components like landing gear, wing roots, arrester devices and engine mountings [1]. For aerospace applications, the feasibility of fabrication of 3.96 m (156 inch) diameter [2] and 6.6 m (260 inch) diameter [3] solid rocket motor cases out of maraging steel has been demonstrated.

The design of a rocket motor case fabricated out of a high strength alloy steel such as maraging steel will be a fracture based one, for which input data on crack size, gross section area stress, fracture mode and detectable flaw sizes by available non-destructive testing (NDT) techniques are essential. In order to gain sufficient experience in using the steel for large size booster cases and to obtain a few design parameters, a sub-scale motor case was designed and fabricated out of 18 nickel 1800 MNm^{-2} maraging steel and burst tested. This paper highlights the investigation on the failure analysis and fracture characteristics of the burst tested rocket motor case and throws light on the capability of 18 nickel 1800 MNm^{-2} maraging steel to withstand the proof pressure. Details of crack length and depth based on fracture mechanics considerations are also presented.

2. Experimental procedure

18 nickel 1800 MNm^{-2} grade maraging steel sheet of 0.0015 m thickness was used to fabricate a 0.3 m diameter, 2 m long motor case. The details of fabrication have been reported elsewhere [4]. Briefly, the motor case was fabricated by tungsten inert gas (TIG) welding, on the solution treated sheets along the length and circumferentially with the domes. The case was aged at 750 K for 3 h before being subjected to pressure testing. Tap water was used as the medium for pressurizing to 12.2 MPa (in steps of 2 MPa and holding for just enough time to complete the strain recordings) and this was repeated for 5 cycles. During the sixth cycle the motor case was pressurized till bursting, which occurred at 15.2 MPa [5]. The hoop stress for this case, based on von Mises theory, and tensile strength was 1754.2 MNm^{-2} [6]. The design stress was known to be about 60 to 70% of the yield stress but strain measurements during the actual test were used to arrive

0022–2461/85 $03.00 + .12

Figure 1 Maraging steel motor case (0.3 m in diameter, 2 m long, 0.0015 m thick). (A) Propulsion cylinder, (B) stub cylinder, (C) nozzle end.

at the correct values. Twenty-three strain gauges were mounted at various locations on the motor case to monitor the strain. Fig. 1 shows the fabricated motor case and Figs. 2 to 4 show the burst motor case at various locations. Fig. 5 shows fragments ejected during bursting. Samples taken from the burst motor case were analysed to reveal the metallurgical aspect of the fracture.

Visual observations, optical metallography (OM) and scanning electron microscopy (SEM) were used for the failure analysis. One sample each from the circumferential weld (nozzle end and propulsion cylinder joint) and longitudinal weld (propulsion cylinder) was prepared for OM in the conventional way through cold mounting the samples, grinding, polishing and etching (using Fry's reagent). The microstructures at the weld, heat affected zone (HAZ) and parent metal were recorded at suitable magnifications. SEM observations were made on fragments ejected during the burst test and also on the portion of the weld which remained attached to the chamber.

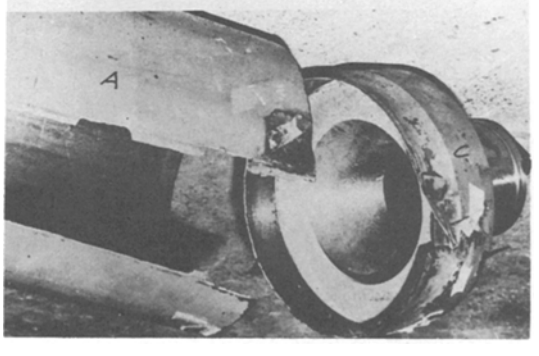

Figure 2 Fracture at the junction between the nozzle end and propulsion cylinder.

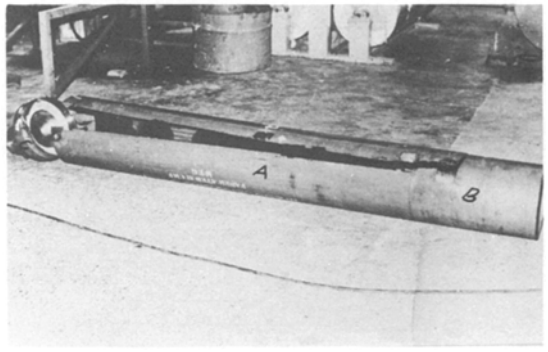

Figure 3 Propulsion cylinder – crack propagation along the longitudinal weld – adjacent to the weld bead.

3. Results and discussion

3.1. Visual observations

Visual inspection of the fabricated motor case revealed that true roundness of the propulsion cylinder was not obtained after its fabrication by press forming. The maximum ovality was measured to be 0.0009 m in the middle. A mismatch of 0.0003 m was seen in the longitudinal and circumferential welds. Fig. 2 shows the fracture surface of the circumferential weld joining the nozzle end and propulsion cylinder. For about 0.2 m of the length the fracture was adjacent to the weld bead. At other places the fracture was 0.005 to 0.008 m away from the weld bead on the propulsion cylinder. Fig. 3 shows that the crack propagation in the propulsion cylinder was all along the longitudinal weld but adjacent to the weld bead. Observation of the inner surface of the chamber revealed that the grinding of the longitudinal weld bead was not complete and there was a step of about 0.0005 to 0.0008 m between the parent metal and weld bead (Fig. 5). This step at the inside portion of the longitudinal

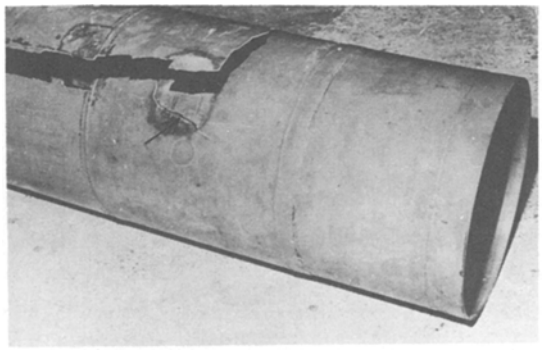

Figure 4 Stub cylinder – tearing.

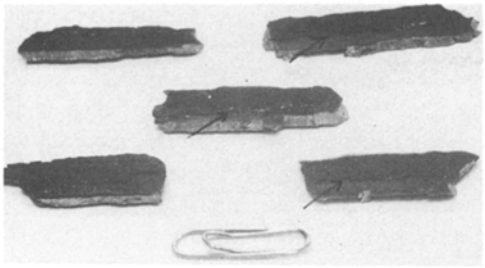

Figure 5 Longitudinal weld fragments of the propulsion cylinder – the step between the parent metal and weld at the inner surface.

weld resulted in non-uniform stresses through the wall thickness [7] and facilitated crack propagation along the longitudinal weld adjacent to the weld bead. In continuation of this longitudinal weld fracture into the stub cylinder (Fig. 4) tearing was seen for about 0.15 m of the length and then the tearing branched out in the circumferential direction for about 0.1 m. It was reasonable to assume that there could be no residual stress in the vessel nor discontinuity stresses at the cylinder/nozzle end dome junction because the entire fabrication was done with maraging steel sheets and the nozzle end dome in the solutionized condition (soft martensite) and then the vessel was aged at 750 K for 3 h.

3.2. Optical metallography

Figs. 6 and 7 respectively show the microstructure of the fusion zone in circumferential and longitudinal welds. Fig. 6 reveals finer columnar dendritic cells, dark etching martensite at the intersection of dendrites and a small quantity of austenite uniformly distributed. Fig. 7 represents the fusion zone in the case of double pass welding and ageing

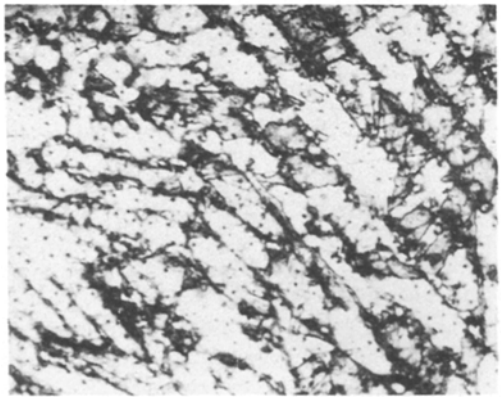

Figure 6 Circumferential weld – fusion zone (OM) (480 ×).

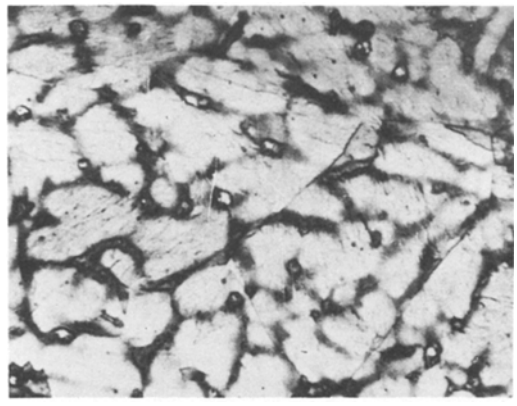

Figure 7 Longitudinal weld – fusion zone (OM), (480 ×).

and reveals coarser columner dendritic cells, with dark etching martensite and non-uniformly distributed austenite. The microstructural features for the HAZ and parent metal for the above two cases do not differ very much from each other. The ductility of the material in the welded condition (as measured by percentage elongation) was 2 to 3%. The other mechanical properties for the above two cases of welding did not change appreciably. Also there was no degradation in mechanical properties due to welding [4].

3.3. SEM

SEM observations of the fracture surface of all sample pieces taken along the longitudinal weld showed equiaxed dimples (Fig. 8), typical of tensile overload failure resulting from microvoid coalescence [7]. The fracture surface of the sample

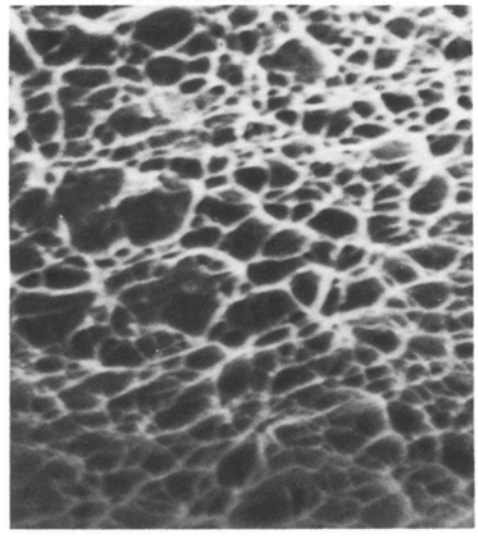

Figure 8 Fracture surface – equiaxed dimples (SEM) (750 ×).

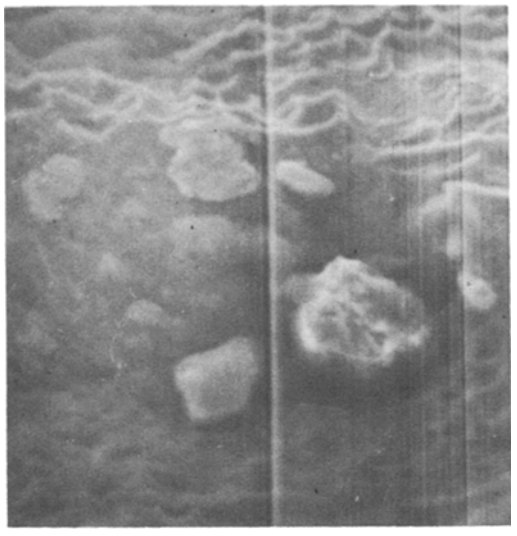

Figure 9 Fracture surface at the circumferential weld at the nozzle end – silicate inclusions (SEM) (750 ×).

taken from the circumferential weld revealed, in addition to dimples, the presence of small inclusions (Fig. 9), which on energy-dispersive X-ray analysis (EDAX) analysis were shown to contain silicon and thus inferred to be silicates. The fracture initiation was from the circumferential weld area and hence these silicate inclusions with the depleted metal zone around probably hepled microvoid formation and subsequent coalescence during the test resulting in an equiaxed dimple structure.

Failure analysis involving visual, OM and SEM observations confirmed that the crack initiation was from silicate inclusions in the circumferential weld at the nozzle end, crack propagation in the propulsion cylinder was along the longitudinal weld adjacent to the weld bead due to non-uniform stresses caused by the step (Fig. 5), and that the longitudinal weld fracture of propulsion cylinder continued into the stub cylinder resulting in tearing.

4. Burst pressure calculations

The pressure required for bursting the motor case P, was calculated as [8]

$$P = \frac{2t\eta\sigma_u}{D \times WM \times BG} \qquad (1)$$

where t is the thickness of motor case (0.0015 m), η is weld efficiency (0.95), σ_u is ultimate tensile strength (1764 MNm^{-2}), D is diameter of motor case (0.3 m), WM is weld mismatch (0.0003 m) and BG is biaxial gain (0.895). The biaxial mechanical properties of metallic sheets are higher than the respective properties in the uniaxial field. The percentage of strength gain so obtained is called the BG of the material. A simple method, which is followed in the present case, of estimating BG for maraging steel which has a close proximity between the yield and ultimate tensile strength, is by using the properties from uniaxial and biaxial stress–strain curves based on major principal strains [9]. This method yielded BG = 0.895 for the present case. From the experimental data shown in brackets, burst pressure was calculated to be 14.9 MPa whereas the motor case actually gave way at 15.2 MPa. Calculations based on von Mises theory [6], showed the effective hoop stress for the above test to be 1754.2 MNm^{-2} as against 1764 MNm^{-2}, the ultimate tensile strength (UTS) of the material in the solution treated and aged condition. Therefore it is inferred that the motor case has satisfactorily withstood the proof pressure test and has given way only at an effective stress almost equal to the UTS of the material.

5. Fracture mechanics considerations

The strain measurements during the proof pressure test revealed that the material behaved linear up to stresses of about 75% of UTS [5], and hence it was appropriate to use linear elastic fracture mechanics (LEFM) to arrive at fracture parameters. The following exercise based on LEFM considerations for critical size and gross section area stress calculations was to show that no crack growth occurred during proof pressure cycling at 12.2 MPa and that the motor case satisfactorily withstood the proof pressure for 5 cycles.

5.1. Critical crack size calculations

The critical crack depth, a_c, is given by the formula [10, 11]

$$a_c = \frac{\phi^2 - 0.212\,(\sigma/\sigma_y)^2}{1.21\pi\sigma^2} K_{IC}^2 \qquad (2)$$

where ϕ is the elliptical integral of second order, σ is design stress σ_D, K_{IC} is the plane strain fracture toughness. For material acceptance as well as for rocket motor case design calculations, only K_{IC} was used as the basic material property. The strain measurements made during the hydroburst test of the motor case [5] revealed a σ_D of 1176 MNm^{-2} for a proof pressure of 12.2 MPa.

Suppose that the crack size parameters reliably

detectable by a non-destructive method (NDT) are a = crack depth = 0.001 m and half crack length c = 0.002 m, i.e. a/c = 0.5. For an experimental yield strength σ_y of 1715 MN m^{-2}, σ_D = 1176 MNm^{-2}, σ_D/σ_y = 0.68 and when σ_D = UTS = 1764 MNm^{-2}, σ_D/σ_y becomes 1. Thus for a/c = 0.5, σ_D/σ_y = 0.68 and using K_{IC} = 99.3 MNm$^{-3/2}$ [12], Equation 2 gives a_c = 0.0026 m. Also for the same a/c = 0.5 when σ_D/σ_y = 1, a_c becomes 0.0023 m, i.e. both these a_c values are larger than the wall thickness of the present motor case. Therefore if crack growth were to occur during the proof pressure cycle, the crack would have grown into a through-thickness crack and leak would have occurred, instead of fracture. Since the motor case withstood 5 repeated proof pressure cycles at 12.2 MPa, it was concluded that there was no (or minimal) crack growth during proof pressure cycling, and the motor gave way only when the pressure was raised to 15.2 MPa, which is equal to an effective stress of 1754.2 MN m^{-2} [6], close to the UTS (1764 MN m^{-2}) of the material. Keeping in mind the lower limit of flaw size as given by NDT detection and the upper limit as the actual motor case thickness (0.0015 m), a = 0.001 m seems to be acceptable as one crack parameter.

5.2. Gross section area stress

The gross section area stress, σ_g, at failure is given by [10]

$$\sigma_g = \frac{K_c}{(\pi C_c)^{1/2}} \frac{1}{\alpha} \qquad (3)$$

where K_c is the critical stress intensity factor, α is the correction factor and C_c is the half crack length at the onset of unstable crack growth. If σ_g is less than the effective stress corresponding to a proof pressure of 12.2 MPa, catastrophic failure would occur during proof pressure cycling itself. Assuming that NDT cannot reliably detect a crack length $2c$ less than 0.004 m, for α = 1, K_c = 99.3 MNm$^{-3/2}$ [12], σ_g works out to be 1254 MNm^{-2}. That is σ_g is larger than the effective stress corresponding to 12.2 MPa, and hence the motor case was able to withstand 5 repeated cycles of proof pressure at 12.2 MPa. However, on subsequent raising of pressure to 15.2 MPa (effective stress of 1754 MNm^{-2}) during the sixth cycle, the motor case gave way since the effective stress was very close to the UTS (1764 MNm^{-2}) of the material. Also, from the above analysis in Subsections 5.1 and 5.2, the acceptable crack size parameters were a = 0.001 m, $2c$ = 0.004 m, i.e. a/c = 0.5.

5.3. Leak before bursting calculations

The leak before bursting criterion for pressure vessels can be written as [13, 14]

$$\frac{\pi(\sigma/\sigma_f)^2}{1 - 0.5\,(\sigma/\sigma_f)^2} \leqslant \beta_{IC}(1 + 1.4\beta_{IC}^2) \qquad (4)$$

where σ is the applied stress, σ_f is effective yield strength or flow strength, $\beta_{IC} = (K_{IC}/\sigma_y)^2/t$, t is thickness. σ is termed σ_{LB} (stress for leak before bursting) where $a = t$, and from values of K_c [12], σ_f [5], and t, σ_{LB} is obtained as 1764 MN m^{-2} which is equal to the UTS of the material in the present case. Therefore when the pressure was raised to 15.2 MPa, resulting in an effective hoop stress of 1754 MN m^{-2}, almost equal to the UTS of the material, rapid fracturing of the motor case occurred without any chance for a leak before bursting to occur, thus validating the above values of a and c.

6. Conclusions

1. Silicate inclusions at the circumferential weld at the nozzle end initiated the crack. The uneven roundness as revealed by ovality, weld mismatch and the step inside the longitudinal weld in the propulsion cylinder acted as stress raisers for crack propagation.

2. The fracture of the motor case is due to tensile overload as revealed by the equiaxed dimple resulting from microvoid formation and coalescence.

3. The calculated burst pressure from the experimental data was 14.9 MPa whereas the motor case gave way at 15.2 MPa. The effective stress for bursting worked out to be 1754 MN m^{-2}, almost equal to the UTS (1764 MN m^{-2}) of the material.

4. Fracture mechanics considerations using the hydroburst test data imply that the crack size parameters for this case are a = 0.001 m and $2c$ = 0.004 m, i.e. a/c = 0.5.

5. The motor case withstood 5 repeated cycles at 12.2 MPa. Therefore no (or minimal) crack growth has taken place during proof pressure cycling. However, at 15.2 MPa rapid fracturing occurred because the effective hoop stress was 1754 MN m^{-2}, almost equal to the UTS (1764 MN m^{-2}) of the material.

6. σ_{LB} is calculated to be equal to the UTS of

the material in the present case and hence there was no chance for a leak before bursting to occur.

7. Acknowledgements

Grateful acknowledgments are due to the Aerospace Structures Division, Vikram Sarabhai Space Centre, for carrying out the hydroburst tests. The authors wish to thank Mr A. Natarajan for OM and Mr Manickavasagam for SEM analyses. The authors thank Dr Vasant R. Gowariker, Director, VSSC, for his permission to publish the paper.

References

1. "Maraging Steels", (Firth Brown Company/Sheffield Forgemasters Ltd, Sheffield, 1976).
2. W. D. ABBOTT, *Welding J.* **45** (1966) 595.
3. J. E. STRAWLEY and J. B. ESGAR, NASA-TM-X-1194, Lewis Research Centre, Cleveland, Ohio, January 1966).
4. S. ARUMUGHAM, "Development of 18 Ni 250 grade Maraging Steel Rocket Motor Case RH-300", VSSC Technical Report, VSSC:TR:042:82 (November 1982).
5. T. CHELLADURAI, M. S. ANANTHANATARAJAN and B. M. BASHA, "Cyclic Proof Pressure and Hydroburst Test on Maraging Steel Motor Case RH-300", VSSC Technical Report, VSSC/ADDG/ASTR/TT(1)/1983 (January 1983).
6. A. R. ACHARYA, "Application of von Mises Theory for M250 Maraging Steel", Aerospace Structures Division Report, VSSC, Trivandrum, (January 1983) private communication.
7. "Failure Analysis and Prevention," American Society for Metals Handbook, Vol. 10, 8th edn (ASM Ohio, 1975) p. 19.
8. M. SUNDARESAN, "Fundamentals of Rocket Motor Case Design", Launch Vehicle Systems Division Report, LVSD/ADDG/82, VSSC, Trivandrum (April 1982) private communication.
9. C. F. BENJAMIN and R. P. WEI, *J. Spacecraft* **2**(3) (1965) 363.
10. "Fracture – An Advanced Treatise", Vol. VI of "Fracture of Metals", edited by A. Leibowitz, (Academic Press, London and New York, 1969) p. 338.
11. S. T. ROLFE and J. M. BARSOM, "Fracture and Fatigue Control in Structures – Applications of Fracture Mechanics" (Prentice Hall, New York 1977) p. 156.
12. V. DIWAKAR and S. ARUMUGHAM, "Fracture Toughness of 18Ni 250 Grade Maraging Steel", VSSC Technical Report VSSC:TR:003:83 (January 1983).
13. G. R. IRWIN, J. M. KRAFT, P. C. PARIS and A. A. WELLS, "Basic Aspects of Crack Growth and Fracture, Reaction Pressure Vessel Technology", edited by G. D. Whitman, G. C. Robinson and A. W. Savolainen, ORNL-NSIC-21, Oak Ridge National Laboratory, Oak Ridge, TN (December 1967) pp. 430–538.
14. G. R. IRWIN and ROLAND deWIT, *J. Testing Evaluation* **11** (1) (January 1983) 56.

Received 23 February
and accepted 4 June 1984